Received: 9 June 2020 | Revised: 21 July 2020 | Accepted: 27 July 2020

DOI: 10.1002/qua.26437

FULL PAPER

International Journal of QUANTUM CHEMISTRY WILEY

On the ^{13}C-NMR chemical shift anisotropy patterns and aromatic character in strained fullerenes: Computational analysis of D_{6h}/D_{2d}-C_{36} fullerene

Raul Guajardo-Maturana[1] | Peter L. Rodríguez-Kessler[2] | Desmond MacLeod-Carey[2] | Alvaro Muñoz-Castro[2]

[1]Facultad de Ciencias de la Salud, Instituto de Investigación Interdisciplinar en Ciencias Biomédicas SEK (I3CBSEK), Universidad SEK, Santiago, Chile

[2]Grupo de Química Inorgánica y Materiales Moleculares, Facultad de Ingeniería, Universidad Autonoma de Chile, Santiago, Chile

Correspondence
Alvaro Muñoz-Castro, Grupo de Química Inorgánica y Materiales Moleculares, Facultad de Ingeniería, Universidad Autonoma de Chile, El Llano Subercaseaux 2801, Santiago, Chile.
Email: alvaro.munoz@uautonoma.cl

Funding information
Fondecyt, Grant/Award Numbers: 1180683, 3190329

Abstract

The NMR characterization of small C_{36} hollow fullerene exposes a stable cage with structural features based on its strained curved π-surface in a D_{6h}-symmetry. Our results indicate that planar-like aromatic properties of the D_{6h}-C_{36} isomer decrease to a nonaromatic cage for D_{2d}-C_{36} after Stone-Wales transformation of an equatorial [6.6] bond. This is given by the decrease of conjugation in the strained π-surface after Stone-Wales transformation. Calculated nuclear shielding shows that the main shielding component is always oriented perpendicularly to the cage π-surface despite the larger curvature degree, as a result of the sp^2 character of carbon atoms, resembling C_{60}. Moreover, the D_{6h}- and D_{2d}-C_{36} cages differ in their charge distribution properties, leading to charge accumulation in the strained cap of the former that leads to a polymerization-prone cage, which contrasts with that expected for the D_{2d} structure. Hence, structural rearrangements of these non-Hirsch aromatic fullerenes show that their inherent global behavior requires considering the structural features besides electron counting rules.

KEYWORDS

aromatic, fullerene, magnetic field, NMR

1 | INTRODUCTION

Fullerenes are a fascinating class of all-carbon molecules compromising a plethora of versatile spherical-shaped architectures.[1–4] Due to their unique structures and properties, fullerenes exhibit various activities and hence have attracted considerable attention for the past few decades.[5–8] With the landmark characterization of buckminsterfullerene (C_{60}),[9] a rapid and extensive growth has been achieved in this field, leading to interdisciplinary applications of technological interest.[5–8,10–13] The spherical aesthetic structure of the prominent C_{60} fullerene obeys the isolated-pentagon rule with a characteristic curved π-system with carbon π-orbitals perpendicular to the spherical surface.[14]

C_{36} is the first stable hollow fullerene composed of a small number of carbon atoms to be characterized, produced by Zettl and coworkers,[15,16] which exhibits an enhanced curved π-system, allowing us to study the characteristics of strained fullerenes as given by low-nuclear cages.[17–25] Recently, C_{36} has served to evaluate the spin gap in supramolecular complexes[26] and the role of symmetry breaking in a single-determinant representation of the electronic structure quantifying the role of electronic correlation[27] by the Lee group. In addition, Song and coworkers extended the studies of C_{36} to the characterization of several isomers by simulating their X-ray photoelectron spectroscopy and near-edge X-ray absorption fine-structure spectra, through density functional theory,[28] as a relevant approach toward the estimation of expected patterns for the characterization of molecular structures of smaller and medium-sized fullerenes. Moreover, the optical absorption characteristics of

C_{36}, and related carbon-nanotubes composites and endohedral counterparts, have been evaluated with regard to the formation of nanostructures materials involving this small cage.[29–33]

The obtained ^{13}C-NMR spectrum shows three different types of carbon atoms accounting for a D_{6h} structure (Figure 1). This prolate carbo-cage is made from 8 six-membered rings, where two of them are located above and below faces, while the other six forms a [6]cyclacene-like middle section barrel shape. In addition, 12 five-membered rings are formed between the above and below rings and the middle section. As a result, C_{36} exhibits the bending of the planar π-system,[14] with a pyramidalization angle (θ*p*) increasing from C3 to C1. Subsequent studies suggest the capabilities to form polymeric structures in the C_{36} solid.[34]

^{13}C-NMR spectroscopy is proven to be effective in achieving detailed characterization of fullerenes in both the solution and the solid states.[16,35–38] Owing to its symmetry, C_{60} shows a single peak at 143.15 ppm at room temperature,[39] where, from the solid state at 77 K, the chemical shift anisotropy (CSA) pattern[37,40,41] is obtained, enabling valuable information reflecting nonaxial symmetry of the chemical environment at the probe nuclei.[42]

The structure of C_{36} retains several five- and six-membered rings confined in a small cage, resulting in a situation, which confronts a different shielding response from each constituent rings, in a curved π-surface. Herein, we elucidate the induced magnetic field in the singlet state of D_{6h}-C_{36}, by means of magnetic response maps, in order to extend our understanding of the behavior of strained cyclic structures and the contribution of each section of the overall magnetic response. Here, we aimed to explore the local and overall magnetic properties of D_{6h}-C_{36}, describing the orientation of the CSA and the induced magnetic field ($\boldsymbol{B}^{ind}$) to extend the understanding of the axis-dependent character of the magnetic behavior of such prominent spherical structures. The determination of CSA tensor[43] provides valuable information concerning the local structural and electronic properties, which are very sensitive to their respective chemical environment. In addition, the evaluation of $\boldsymbol{B}^{ind}$ offers an overall picture of the shielding and deshielding regions through space, which has been extensively used to understand the global aromatic behavior of three-dimensional aromatic molecules.[44–46]

2 | COMPUTATIONAL DETAILS

Geometry optimizations and subsequent calculations were performed by using DFT methods utilizing the ADF 2016 code[47] with the all-electron triple-ξ Slater basis set plus the double-polarization (STO-TZ2P) basis set in conjunction with the Becke-Perdew (BP86) functional within the generalized gradient approximation (GGA).[48,49] The molecular shielding tensor[50] at several points of the molecular domain was calculated within the gauge-independent atomic orbital (GIAO) formalism, using the GGA exchange expression proposed by Handy and Cohen[51] and the correlation expression proposed by Perdew, Burke, and Ernzerhof[52] and the all-electron STO-TZ2P basis set. ^{13}C-NMR chemical shift calculations are given relative to tetramethylsilane (TMS), according to $\delta^C = \sigma^S - \sigma^C$, where σ^S = 192.3 ppm.

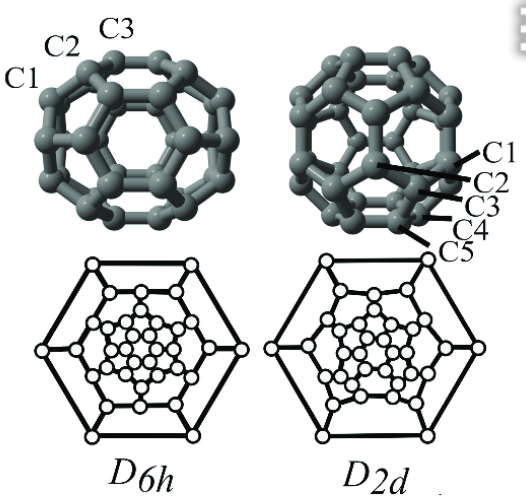

FIGURE 1 Structures for D_{6h}-C_{36} and D_{2d}-C_{36}, and their respective Schlegel diagram. Representative atoms are denoted

3 | RESULTS AND DISCUSSION

The hollow C_{36} fullerene has been depicted to have a barrel shape with a D_{6h} symmetry, as suggested by the characterized ^{13}C-NMR spectrum, denoting three distinctive signals showing a singlet-state D_{6h}-C_{36} fullerene.[16] Computational studies on C_{36} determine the existence of 15 isomers, from where the D_{6h} and D_{2d} structures represent the most stable counterparts owing to their minimal number of adjacent pentagonal faces (Figure 1).[14,53,54] Both D_{6h} and D_{2d} isomers are connected through a Stone-Wales transformation of an equatorial [6.6] bond, as discussed previously by Jin and Hao.[55] Here, we focus on their electronic singlet state to make a comparison in relation to C_{60}.

D_{6h}-C_{36} depicts three different carbon atoms (Figure 1), in a prolate cage showing 6 six-membered rings as a [6]cyclacene-like middle section, capped by two motifs formed by 6 five-membered rings surrounding a six-membered face. As a result, C_{36} exhibits an increasing bending of the π-surface from C3 to C1, with pyramidalization angles[56] θp = (θ$_{\sigma\pi}$-90)° of 12.6°, 15.4°, and 17.4°, respectively. For D_{2d}-C_{36}, 8 six-membered rings result into two separate tetracene-like fused motifs, leaving 12 five-membered rings. As a consequence of the decreasing symmetry, five carbon atom types are found for D_{2d}-C_{36}, showing a θp of 13.0°, 12.5°, 15.8°, 17.4°, and 15.8° for C1 to C5, respectively. Such values are indicative of more curved sections on the C_{36} surface, in relation to C_{60} (θp = 11.6). The curvature at C3 of D_{6h}-C_{36} is similar to C_{60}, increasing for C2- and C1-, indicative of the more curved section at the top and bottom of the structure. For the D_{2d}-isomer, C1 and C2 show similar θp to C_{60}, with an increasing pyramidalization angle indicating a larger curvature for C3 to C5 atoms.

The calculated ^{13}C-NMR parameters for D_{6h}-C_{36} show three different carbon types with an isotropic chemical shift (δ_{iso}) amounting to 157.8 ppm for the more strained carbon (C1), 152.9 ppm for C2, and 136.2 ppm for C3, which are in line with the values observed experimentally and discussed by earlier calculations in the experimental report of Zettl, with values of double intensity for the 146.1 ppm peak and a single intensity peak at 137.5 ppm.[16] The difference observed for peaks of C1 and C2 has been attributed to additional shielding given by neighboring molecules or paramagnetic impurities.[16] Moreover, D_{2d}-C_{36} can be described by five unique carbon atoms expected at 149.2 (C1), 149.8 (C2), 152.9 (C3), 134.0 (C4), and 134.6 (C5) ppm (Table 1).

The graphical representation of the absolute shielding (σ_{ij}, i, j = 1, 2, 3) accounts for the orientation, magnitude, and sign of the local response at each carbon center in relation to its own principal axis system[43] (Figure 2), which are later reduced to a single value owing to the molecular tumbling in solution. The main shielding component, denoted as σ_{33} or δ_{33}, for absolute shielding and chemical shift representation, respectively, is always oriented perpendicularly to the cage π-surface as a result of the sp^2 character of carbon atoms, which is similar to C_{60},[42] despite the

TABLE 1 Calculated ^{13}C-NMR pattern for D_{6h}- and D_{2d}-C_{36} fullerenes (values in ppm)

	δ_{11}	δ_{22}	δ_{33}	δ_{iso}
D_{6h}-C_{36}				
C1	245.5	192.6	35.3	157.8
C2	247.1	144.5	67.2	152.9
C3	235.5	137.3	35.7	136.2
D_{2d}-C_{36}				
C1	218.3	199.8	29.5	149.2
C2	207.9	206.9	34.6	149.8
C3	243.3	159.9	55.5	152.9
C4	223.1	161.1	17.7	134.0
C5	218.2	135.1	50.5	134.6

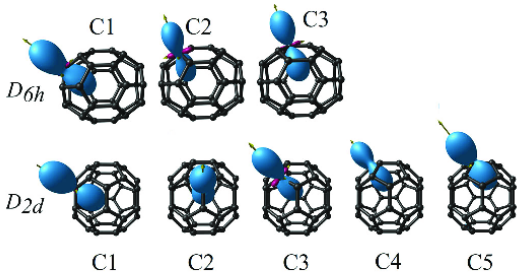

FIGURE 2 Orientation and magnitude of the CSA tensor for representative carbon atoms for D_{6h}-C_{36} and D_{2d}-C_{36}. The orientation of the main shielding component, denoted as σ_{33} or δ_{33}, is shown by the yellow arrow. CSA, chemical shift anisotropy

larger curvature degree. The δ_{22} and δ_{11} components are contained mainly in the D_{6h}-C_{36} surface, with the most deshielded component contained in the [5.5] C—C bonds for C1 and C2, [6.6] for C3, and δ_{22} pointing toward the [5.6]. Similar orientations are obtained for D_{2d}-C_{36}. In contrast, in C_{60}, δ_{22} is the only component located along a C—C bond oriented through the [6.6] bond, owing to the more strained structure in the smaller C_{36} fullerenes.

In order to evaluate the induced magnetic field of D_{6h}- and D_{2d}-C_{36} structures, we obtained the graphical representation of the molecular response ($\boldsymbol{B}^{ind}$) to an external magnetic field ($\boldsymbol{B}^{ext}$),[57,58] given the generalization of nucleus-independent shielding tensor (σ_{ij}), as $\boldsymbol{B}_i^{ind} = -\sigma_{ij}\,\boldsymbol{B}_j^{ext}$ in the molecular domain. This provides a visualization of the induced magnetic field in relation to different orientations of the externally applied field, as well as their averaged (isotropic) representation, providing a global picture of the shielding and deshielding regions, where the *i* and *j* suffices are related to the x-, y-, and z-axis of the molecule-fixed Cartesian system (*i*,*j* = x,y,z). This results in the understanding of the aromatic characteristics in terms of a global property inherent to the molecular structure instead of the local behavior of each aromatic ring, which is influenced by local effects of curvature and fused ring effects.

The isotropic response given by B_{iso}^{ind} (Figure 3) accounts for the experimental molecular tumbling in solution NMR experiments, denoting a strong shielding region (>−20 ppm) at the center of the structure and a shielding surface of −2 ppm following the carbon backbone for the D_{6h}-C_{36} structure. In contrast to the D_{2d}-C_{36} isomer, after a Stone-Wales transformation, the deshielding region is located at the five-membered rings, which diminishes the central shielding region, highlighting the role of the cage arrangement in the resulting property. This difference is given by the [6]cyclacene-like middle section in D_{6h}-C_{36}, which faces several aromatic rings, which builds up a stronger shielding region inside such a cage.

Under certain orientations of the field, the magnetic complexity in these strained fullerenes is evaluated. In this sense, the B_z^{ind} component accounts for a perpendicular applied field in relation to the [6]cyclacene-like middle section of D_{6h}-C_{36}, which reveals a long-ranged shielding region complemented by a perpendicular deshielding region, accounting for the shielding cone property under such orientation. This suggests the formation of π-aromatic circuits perpendicular to the z-axis. In contrast, under a field along both x- and y-axes, given by B_x^{ind} and B_y^{ind}, respectively, the shielding cone property is not found, resulting in a short-ranged response involving shielding regions at six-membered rings and deshielding at pentagons.[59] This suggests that D_{6h}-C_{36} behave as a planar-like aromatic species, where the excess of four electrons from the expected 32-π spherical Hirsch aromatic cage ($2[N + 1]^2$, $N = 3$)[60] hampers the possible spherical aromatic character. As a result, the calculated NICS(0) values[61] at the center of the D_{6h}-C_{36} cage of −26.3 ppm indicates the discussed aromatic character.

For D_{2d}-C_{36}, under different orientations of the field, no shielding cone is sustained, ascribing this isomer as a nonaromatic cage. From B_z^{ind}, a local aromatic character from aromatic hexagons is denoted. This observation shows the critical role of structural rearrangements in determining aromatic properties of these non-Hirsch aromatic species, where the Stone-Wales transformation of an equatorial [6.6] bond in the D_{6h}-C_{36} fullerene reduces the conjugation along the strained π-surface, which should be taken into account besides the electron counting rules. As a result, the calculated NICS(0) values[61] at the center of the D_{2d}-C_{36} cage decreases the central shielding to −11.2 ppm, indicating the decrease in the aromatic character of the overall cage. Moreover, aromaticity in doped-C_{36} species have been discussed in the literature.[62]

An evaluation of the charge distribution along the structure is given by the electrostatic potential map in Figure 4. For the D_{6h} cage, large charge accumulation is found at the [5,6] bonds of the six fused pentagon caps, resulting in a reactive site for further polymerization, as discussed previously.[34] For the D_{2d} isomer, the charge accumulation is distributed along the overall cage, suggesting that the polymerization capabilities

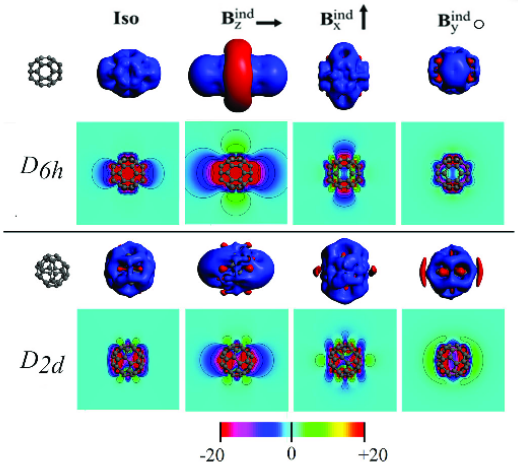

FIGURE 3 Three-dimensional and cut-plane representation of the magnetic response B^{ind} in relation to the orientationally averaged external field (iso, B_{iso}^{ind}) and specific orientations of the applied field (B_i^{ind}; *i* = *x*, *y*, *z*). Isosurface values set at 2 ppm relative to the external field

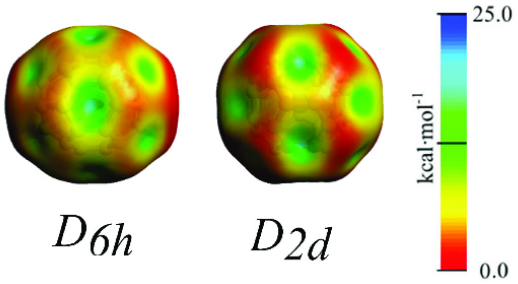

FIGURE 4 Electrostatic potential maps of D_{6h}- and D_{2d}-C_{36}, mapped on isosurfaces of 0.001 a.u. of electron density

are decreased in comparison to the barrel-like D_{6h} structure, where [5,6] bonds carry more charge than [5,5] and [6,6] C—C bonds, resulting in a more delocalized charge.

4 | CONCLUSIONS

In conclusion, our study reveals the magnetic response properties of the smaller characterized hollow fullerene C_{36} to be highly sensitive to the structural arrangement of the cage. For the D_{6h}-isomer, characterized experimentally by ^{13}C-NMR, a planar-like aromatic behavior is observed where the extra four electrons from the expected spherical aromatic 32-π species hamper a possible spherical aromatic character. After the Stone-Wales transformation of an equatorial [6.6] bond leading to D_{2d}-C_{36}, a no-shielding cone property is obtained, ascribing this isomer as a nonaromatic cage. This is given by the decrease of conjugation in the strained π-surface after Stone-Wales transformation. The aromatic characteristics in terms of a global property are inherent to the molecular structure instead of evaluating a local behavior for each aromatic ring. Moreover, the D_{6h}- and D_{2d}-C_{36} cages differ in their charge distribution properties, where the more strained cap of the former results in a localized charge accumulation, leading to a polymerization-prone cage, in contrast to the expected properties for D_{2d}. Thus, structural rearrangements of non-Hirsch aromatic fullerenes are relevant to determine the global behavior of the carbo-cage, which should be taken into account besides electron-counting rules.

ACKNOWLEDGMENTS

The author is grateful for the financial support of FONDECYT Grant 1180683 (Alvaro Muñoz-Castro) and FONDECYT Postdoctorado 3190329 (Peter L. Rodríguez-Kessler).

AUTHOR CONTRIBUTIONS

Alvaro Muñoz-Castro: Conceptualization; data curation; formal analysis; funding acquisition; investigation; methodology; project administration; visualization; writing-original draft; writing-review and editing. **Raul Guajardo:** Data curation; formal analysis; visualization; writing-original draft; writing-review and editing. **Desmond MacLeod Carey:** Formal analysis; funding acquisition; supervision; visualization; writing-original draft; writing-review and editing. **Peter Rodríguez-Kessler:** Conceptualization; visualization; writing-original draft; writing-review and editing.

ORCID

Desmond MacLeod-Carey https://orcid.org/0000-0003-4261-3684
Alvaro Muñoz-Castro https://orcid.org/0000-0001-5949-9449

REFERENCES

[1] K. M. Kadish, R. S. Ruoff, *Fullerenes: Chemistry, Physics, and Technology*, John Wiley & Sons Ltd, New York, NY **2000**.
[2] M. Murata, Y. Murata, K. Komatsu, *Chem. Commun*. **2008**(46), 6083.
[3] P. Schwerdtfeger, L. N. Wirz, J. Avery, *Wiley Interdiscip. Rev. Comput. Mol. Sci*. **2015**, *5*, 96.
[4] M. A. Petrukhina, L. T. Scott, *Fragments of Fullerenes and Carbon Nanotubes*, John Wiley & Sons, Inc, Hoboken, NJ **2011**.
[5] R. O. Loutfy, S. Katagiri, in *Perspectives of Fullerene Nanotechnology* (Ed: E. Ösawa), Springer, Dordrecht, the Netherlands **2002**, p. 357.
[6] X. Lu, L. Feng, T. Akasaka, S. Nagase, *Chem. Soc. Rev*. **2012**, *41*, 7723.
[7] A. Montellano, T. Da Ros, A. Bianco, M. Prato, *Nanoscale* **2011**, *3*, 4035.
[8] M. Prato, *J. Mater. Chem*. **1997**, *7*, 1097.
[9] H. W. Kroto, J. R. Heath, S. C. O'Brien, R. F. Curl, R. E. Smalley, *Nature* **1985**, *318*, 162.
[10] H. Kawabata, H. Tachikawa, *Jpn. J. Appl. Phys*. **2019**, *58*, 121001.

[11] S. Yoshizawa, S. Abe, M. Mutoh, T. Kusaka, M. Nakamura, Y. Yoshida, J. Iida, H. Kawabata, H. Tachikawa, *Jpn. J. Appl. Phys.* **2017**, *56*, 01AE03.
[12] H. Tachikawa, H. Kawabata, *Jpn. J. Appl. Phys.* **2016**, *55*, 02BB01.
[13] E. Durgun, S. Ciraci, T. Yildirim, *Phys. Rev. B* **2008**, *77*, 085405.
[14] X. Lu, Z. Chen, *Chem. Rev.* **2005**, *105*, 3643.
[15] C. Piskoti, A. Zettl, *AIP Conf. Proc.* **1998**, *442*, 183.
[16] C. Piskoti, J. Yarger, A. Zettl, *Nature* **1998**, *393*, 771.
[17] S. Abe, S. Kawano, Y. Toida, M. Nakamura, S. Inoue, H. Sano, Y. Yoshida, H. Kawabata, H. Tachikawa, *Jpn. J. Appl. Phys.* **2016**, *55*, 03DD03.
[18] H. Kawabata, H. Tachikawa, *J. Carbon Res.* **2017**, *3*, 15.
[19] D. Zhao, S. Liu, C. Rong, A. Zhong, S. Liu, *ACS Omega* **2018**, *3*, 17986.
[20] S. A. Siadati, E. Vessally, A. Hosseinian, L. Edjlali, *Synth. Met.* **2016**, *220*, 606.
[21] E. Vessally, S. A. Siadati, A. Hosseinian, L. Edjlali, *Talanta* **2017**, *162*, 505.
[22] T. Tawar, A. Kerim, *Fuller. Nanotub. Carbon Nanostruct.* **2015**, *23*, 846.
[23] X.-Y. Hou, A. Kerim, *J. Theor. Comput. Chem.* **2016**, *15*, 1650057.
[24] A. Abdukadir, A. Kerim, K. Omar, L. Hushur, *Fuller. Nanotub. Carbon Nanostruct.* **2016**, *24*, 662.
[25] T. Iyama, S. Abe, H. Tachikawa, *Mol. Cryst. Liq. Cryst.* **2012**, *567*, 200.
[26] J. Lee, F. D. Malone, M. A. Morales, *J. Chem. Theory Comput.* **2020**, *16*, 3019.
[27] J. Lee, M. Head-Gordon, *Phys. Chem. Chem. Phys.* **2019**, *21*, 4763.
[28] Y. Ma, J.-R. Zhang, S.-Y. Wang, J. Hu, J. Lin, X.-N. Song, *Mol. Phys.* **2019**, *117*, 635.
[29] A. V. Silant'ev, *Russ. Phys. J.* **2019**, *62*, 925.
[30] K. Srinivasu, M. Sundararajan, *J. Chem. Sci.* **2017**, *129*, 783.
[31] K. S. Grishakov, K. P. Katin, M. M. Maslov, *Adv. Phys. Chem.* **2016**, *2016*, 1.
[32] D. Manna, T. K. Ghanty, *J. Phys. Chem. C* **2013**, *117*, 17859.
[33] S.-W. Tang, F.-D. Wang, Y.-H. Li, F. Wang, S.-B. Yang, H. Sun, Y.-F. Chang, R.-S. Wang, *J. Mol. Model.* **2013**, *19*, 5579.
[34] J. C. Grossman, S. G. Louie, M. L. Cohen, *Phys. Rev. B* **1999**, *60*, R6941.
[35] J. Kaminský, M. Buděšínský, S. Taubert, P. Bouř, M. Straka, *Phys. Chem. Chem. Phys.* **2013**, *15*, 9223.
[36] T. Heine, M. Bühl, P. W. Fowler, G. Seifert, *Chem. Phys. Lett.* **2000**, *316*, 373.
[37] C. S. Yannoni, R. D. Johnson, G. Meijer, D. S. Bethune, J. R. Salem, *J. Phys. Chem.* **1991**, *95*, 9.
[38] R. Tycko, R. C. Haddon, G. Dabbagh, S. H. Glarum, D. C. Douglass, A. M. Mujsce, *J. Phys. Chem.* **1991**, *95*, 518.
[39] A. G. Avent, D. Dubois, A. Pénicaud, R. Taylor, *J. Chem. Soc. Perkin Trans.* **1997**, *2*, 1907.
[40] A. M. Orendt, J. C. Facelli, S. Bai, A. Rai, M. Gossett, L. T. Scott, J. Boerio-Goates, R. J. Pugmire, D. M. Grant, *J. Phys. Chem. A* **2000**, *104*, 149.
[41] H. Saitô, I. Ando, A. Ramamoorthy, *Prog. Nucl. Magn. Reson. Spectrosc.* **2010**, *57*, 181.
[42] A. Muñoz-Castro, *Chem. Commun.* **2015**, *51*, 10287.
[43] M. J. Duer, *Solid State NMR Spectroscopy: Principles and Applications*, Wiley-Blackwell, New Jersey, USA **2002**.
[44] A. Miralrio, L. E. L. E. Sansores, B. King, A. Muñoz-Castro, *Phys. Chem. Chem. Phys.* **2018**, *20*, 26325.
[45] A. Muñoz-Castro, *Phys. Chem. Chem. Phys.* **2018**, *20*, 3433.
[46] A. Muñoz-Castro, *Phys. Chem. Chem. Phys.* **2017**, *19*, 12633.
[47] *Amsterdam Density Functional (ADF 2016) Code*. Vrije Universiteit, Amsterdam, The Netherlands, http://www.scm.com.
[48] J. P. Perdew, *Phys. Rev. B* **1986**, *33*, 8822.
[49] A. D. Becke, *Phys. Rev. A* **1988**, *38*, 3098.
[50] S. K. Wolff, T. Ziegler, E. van Lenthe, E. J. Baerends, *J. Chem. Phys.* **1999**, *110*, 7689.
[51] N. C. Handy, A. J. Cohen, *Mol. Phys.* **2001**, *99*, 403.
[52] J. P. Perdew, K. Burke, M. Ernzerhof, *Phys. Rev. Lett.* **1997**, *78*, 1396.
[53] E. E. B. Campbell, P. W. Fowler, D. Mitchell, F. Zerbetto, *Chem. Phys. Lett.* **1996**, *250*, 544.
[54] P. W. Fowler, T. Heine, *J. Chem. Soc. Perkin Trans.* **2001**, *2*, 487.
[55] Y. Jin, C. Hao, *J. Phys. Chem. A* **2005**, *109*, 2875.
[56] R. C. Haddon, L. T. Scott, *Pure Appl. Chem.* **1986**, *58*, 137.
[57] R. Islas, T. Heine, G. Merino, *Acc. Chem. Res.* **2012**, *45*, 215.
[58] G. Merino, T. Heine, G. Seifert, *Chem. A Eur. J.* **2004**, *10*, 4367.
[59] A. Kerim, *J. Mol. Model.* **2011**, *17*, 3257.
[60] A. Hirsch, Z. Chen, H. Jiao, *Angew. Chemie* **2000**, *39*, 3915.
[61] Z. Chen, C. S. Wannere, C. Corminboeuf, R. Puchta, P. v. R. Schleyer, *Chem. Rev.* **2005**, *105*, 3842.
[62] P. Abdurishit, A. Kerim, K. Najmidin, H. Kalam, T. Tawar, *Chem. Mon.* **2014**, *145*, 405.

How to cite this article: Guajardo-Maturana R, Rodríguez-Kessler PL, MacLeod-Carey D, Muñoz-Castro A. On the ^{13}C-NMR chemical shift anisotropy patterns and aromatic character in strained fullerenes: Computational analysis of D_{6h}/D_{2d}-C_{36} fullerene. *Int J Quantum Chem*. 2021;121:e26437. https://doi.org/10.1002/qua.26437